

# Measurement of $R$ between 1.84 and 3.05 GeV at the KEDR detector

V.V. Anashin<sup>a</sup>, V.M. Aulchenko<sup>a,b</sup>, E.M. Baldin<sup>a,b</sup>, A.K. Barladyan<sup>a</sup>, A.Yu. Barnyakov<sup>a,b</sup>, M.Yu. Barnyakov<sup>a,b</sup>, S.E. Baru<sup>a,b</sup>, I.Yu. Basok<sup>a</sup>, A.M. Batrakov<sup>a</sup>, A.E. Blinov<sup>a,b</sup>, V.E. Blinov<sup>a,b,c</sup>, A.V. Bobrov<sup>a,b</sup>, V.S. Bobrovnikov<sup>a,b</sup>, A.V. Bogomyagkov<sup>a,b</sup>, A.E. Bondar<sup>a,b</sup>, A.R. Buzykaev<sup>a,b</sup>, S.I. Eidelman<sup>a,b</sup>, D.N. Grigoriev<sup>a,b,c</sup>, Yu.M. Glukhovchenko<sup>a</sup>, S.E. Karnae<sup>a</sup>, G.V. Karpov<sup>a</sup>, S.V. Karpov<sup>a</sup>, P.V. Kasyanenko<sup>a</sup>, T.A. Kharlamova<sup>a</sup>, V.A. Kiselev<sup>a</sup>, V.V. Kolmogorov<sup>a</sup>, S.A. Kononov<sup>a,b</sup>, K.Yu. Kotov<sup>a</sup>, E.A. Kravchenko<sup>a,b</sup>, V.N. Kudryavtsev<sup>a,b</sup>, V.F. Kulikov<sup>a,b</sup>, G.Ya. Kurkin<sup>a,c</sup>, I.A. Kuyanov<sup>a</sup>, E.A. Kuper<sup>a,b</sup>, E.B. Levichev<sup>a,c</sup>, D.A. Maksimov<sup>a,b</sup>, V.M. Malyshev<sup>a</sup>, A.L. Maslennikov<sup>a,b</sup>, O.I. Meshkov<sup>a,b</sup>, S.I. Mishnev<sup>a</sup>, I.I. Morozov<sup>a,b</sup>, N.Yu. Muchnoi<sup>a,b</sup>, V.V. Neufeld<sup>a</sup>, S.A. Nikitin<sup>a</sup>, I.B. Nikolaev<sup>a,b</sup>, I.N. Okunev<sup>a</sup>, A.P. Onuchin<sup>a,b,c</sup>, S.B. Oreshkin<sup>a</sup>, A.A. Osipov<sup>a,b</sup>, I.V. Ovtin<sup>a,c</sup>, S.V. Peleganchuk<sup>a,b</sup>, S.G. Pivovarov<sup>a,c</sup>, P.A. Piminov<sup>a</sup>, V.V. Petrov<sup>a</sup>, V.G. Prisekin<sup>a,b</sup>, O.L. Rezanova<sup>a,b</sup>, A.A. Ruban<sup>a,b</sup>, V.K. Sandryev<sup>a</sup>, G.A. Savinov<sup>a</sup>, A.G. Shamov<sup>a,b</sup>, D.N. Shatilov<sup>a</sup>, B.A. Shwartz<sup>a,b</sup>, E.A. Simonov<sup>a</sup>, S.V. Sinyatkin<sup>a</sup>, A.N. Skrinsky<sup>a</sup>, A.V. Sokolov<sup>a,b</sup>, A.M. Sukharev<sup>a,b</sup>, E.V. Starostina<sup>a,b</sup>, A.A. Talyshv<sup>a,b</sup>, V.A. Tayursky<sup>a,b</sup>, V.I. Telnov<sup>a,b</sup>, Yu.A. Tikhonov<sup>a,b</sup>, K.Yu. Todyshev<sup>a,b,\*</sup>, G.M. Tumaikin<sup>a</sup>, Yu.V. Usov<sup>a</sup>, A.I. Vorobiov<sup>a</sup>, V.N. Zhilich<sup>a,b</sup>, V.V. Zhulanov<sup>a,b</sup>, A.N. Zhuravlev<sup>a,b</sup>

<sup>a</sup>*Budker Institute of Nuclear Physics, 11, akademika Lavrentieva prospect, Novosibirsk, 630090, Russia*

<sup>b</sup>*Novosibirsk State University, 2, Pirogova street, Novosibirsk, 630090, Russia*

<sup>c</sup>*Novosibirsk State Technical University, 20, Karl Marx prospect, Novosibirsk, 630092, Russia*

arXiv:1610.02827v2 [hep-ex] 24 Nov 2016

## Abstract

Using the KEDR detector at the VEPP-4M  $e^+e^-$  collider, we have determined the values of  $R$  at thirteen points of the center-of-mass energy between 1.84 and 3.05 GeV. The achieved accuracy is about or better than 3.9% at most of the energy points with a systematic uncertainty less than 2.4%.

## 1. Introduction

Measurement of the  $R$  value has long history and became a classical experiment on high energy physics. The quantity  $R$  is defined as

$$R = \frac{\sigma(e^+e^- \rightarrow \text{hadrons})}{\sigma(e^+e^- \rightarrow \mu^+\mu^-)}, \quad (1)$$

where  $\sigma(e^+e^- \rightarrow \text{hadrons})$  is the radiatively-corrected total hadronic cross section in electron-positron annihilation and  $\sigma(e^+e^- \rightarrow \mu^+\mu^-)$  is the lowest-order QED cross section of the muon pair production.

The experiments devoted to the  $R$  measurement in the energy range from 1.8 GeV up to the vicinity of  $J/\psi$  are described in Refs. [1, 2, 3, 4, 5, 6, 7]. The accuracy of BES-II results [7] at 2.6 and 3.07 GeV reaches 3.8% and 3.3%, respectively, while the precision in other experiments does not exceed 5%.

Precise measurements of the  $R(s)$  dependence play an important role in the determination of the running strong coupling constant  $\alpha_s(s)$  and heavy quark masses [8], the anomalous magnetic moment of the muon  $(g-2)_\mu$  and the value of the electromagnetic fine structure constant at the  $Z^0$  peak  $\alpha(M_Z^2)$  [9, 10]. A significant contribution to uncertainties of the quantities listed above comes from the energy region below charm threshold, which motivated us to perform new  $R(s)$  measurements.

KEDR has recently published the  $R$  values at seven points of the center-of-mass energy between 3.12 and 3.72 GeV [11]. In this paper we present  $R(s)$  measurements in the energy range

from 1.84 GeV up to 3.05 GeV. The experiment with an integrated luminosity of about 0.66 pb<sup>-1</sup> was carried out in 2010. Our result considerably improves the existing  $R(s)$  measurements in this energy range and would be useful for matching CMD-3 and SND data which will be obtained by summing cross sections of the exclusive modes.

## 2. VEPP-4M collider and KEDR detector

The  $e^+e^-$  collider VEPP-4M [12] can operate in the 2×2 bunches mode in the wide range of the beam energy. The peak luminosity of VEPP-4M is about 10<sup>30</sup> cm<sup>-2</sup>s<sup>-1</sup> in the vicinity of  $J/\psi$  and drops to 10<sup>29</sup> cm<sup>-2</sup>s<sup>-1</sup> at the beam energy of 1 GeV.

The VEPP-4M is equipped with two systems of beam energy calibration. The resonant depolarization method [13, 14] is used for precise mass measurements [15, 16]. In experiments requiring long-term data collection the energy monitoring is performed with the infrared light Compton backscattering (CBS) [17].

A detailed description of the KEDR detector can be found in Ref. [18]. Charged particles are reconstructed by the drift chamber (DC) and vertex detector (VD) which compose the tracking system of the detector. Electrons are identified by the ratio of the energy deposited in the CsI and LKr calorimeters to the track momentum. The particle identification system is based on the aerogel Cherenkov counters. The primary trigger (PT) operates using signals from the time-of-flight (TOF) counters and fast signals from the CsI and LKr calorimeters, the secondary trigger (ST) uses optimally shaped calorimeter

\*Corresponding author, e-mail: todyshev@inp.nsk.su

signals and the information from the VD, DC and TOF systems [19]. Muons are identified in the muon system inside the magnet yoke. The superconducting solenoid provides a longitudinal magnetic field of 0.6 T. The detector is equipped with a tagging system of scattered electrons for two-photon studies. The on-line luminosity measurement is provided by two independent single bremsstrahlung monitors.

### 3. Experiment

The purpose of the experiment was the determination of the total hadron cross section at thirteen equidistant points between 1.84 and 3.05 GeV. During data taking there were some problems with the laser for CBS energy measurements. At most points the energy was determined using the correction of the calculated accelerator energy. These corrections were found in the experiment on the narrow resonance search [20]. The accuracy of beam energy determination was about 1 MeV that was checked using a few CBS calibrations performed during the  $R$  scan.

The actual energy and integrated luminosity at all points are presented in Table 1. The systematic uncertainty in the measured integrated luminosity is considered in Sec. 5.1.

Table 1: Center-of-mass energy  $\sqrt{s}$  and integrated luminosity  $\int \mathcal{L} dt$  in the  $R$  scan points.

Point	$\sqrt{s}$ , MeV	$\int \mathcal{L} dt$ , nb $^{-1}$
1	1841.0	$10.32 \pm 0.19 \pm 0.12$
2	1937.0	$29.13 \pm 0.34 \pm 0.35$
3	2037.3	$43.16 \pm 0.44 \pm 0.52$
4	2135.7	$43.29 \pm 0.46 \pm 0.52$
5	2239.2	$46.40 \pm 0.49 \pm 0.56$
6	2339.5	$54.55 \pm 0.56 \pm 0.65$
7	2444.1	$52.80 \pm 0.57 \pm 0.63$
8	2542.6	$52.13 \pm 0.59 \pm 0.63$
9	2644.8	$55.43 \pm 0.64 \pm 0.67$
10	2744.6	$66.80 \pm 0.72 \pm 0.80$
11	2849.7	$69.14 \pm 0.77 \pm 0.83$
12	2948.9	$75.87 \pm 0.83 \pm 0.91$
13	3048.1	$60.08 \pm 0.76 \pm 0.72$

## 4. Data analysis

### 4.1. Analysis procedure

The observed hadronic annihilation cross section was determined from

$$\sigma_{\text{obs}}(s) = \frac{N_{\text{h}} - N_{\text{res.bg.}}}{\int \mathcal{L} dt}, \quad (2)$$

where  $N_{\text{h}}$  is the number of events that meet hadronic selection criteria,  $N_{\text{res.bg.}}$  is the residual machine background evaluated as discussed in Sec. 4.6, and  $\int \mathcal{L} dt$  is the integrated luminosity.

For the given observed cross section, the  $R$  value was calculated as follows:

$$R = \frac{\sigma_{\text{obs}}(s) - \sum \varepsilon_{\text{bg}}(s) \sigma_{\text{bg}}(s)}{\varepsilon(s) (1 + \delta(s)) \sigma_{\mu\mu}(s)}, \quad (3)$$

where  $\sigma_{\mu\mu}(s) = 4\pi\alpha^2/3s$  is the Born cross section for  $e^+e^- \rightarrow \mu^+\mu^-$ , and  $\varepsilon(s)$  is the detection efficiency for the single photon annihilation to hadrons. The second term in the numerator corresponds to the physical background from  $e^+e^-$ ,  $\mu^+\mu^-$  production and two-photon processes. The radiation correction factor  $1 + \delta(s)$  can be written as

$$1 + \delta(s) = \int \frac{dx}{1-x} \frac{\mathcal{F}(s, x)}{|1 - \Pi((1-x)s)|^2} \frac{R((1-x)s) \varepsilon((1-x)s)}{R(s) \varepsilon(s)}, \quad (4)$$

where  $\mathcal{F}(s, x)$  and  $\Pi$  are the radiative correction kernel [21] and the vacuum polarization operator, respectively. The variable  $x$  is a fraction of  $s$  lost as a result of initial-state radiation.

The calculation of the radiation correction is presented in detail in Section 4.7.

### 4.2. Monte Carlo simulation

The KEDR simulation program is based on the GEANT package, version 3.21 [22].

Single-photon annihilation to hadrons was simulated using the LUARLW [23] generator, which was employed by the BES collaboration for the high-precision measurement of the  $R$  value [7]. As an alternative, to simulate uds continuum we employed the JETSET 7.4 code [24, 25] with the parameters tuned at energy points 1, 2, 4, 9, 10 and 13.

Bhabha events required for the precise luminosity determination and  $\mu^+\mu^-$  background process were simulated using the MCGPJ generator [26]. To simulate two-photon processes  $e^+e^- \rightarrow e^+e^-X$ , we employed the generators described in Refs. [27, 28, 29].

The results are presented in Fig. 1, where the most important event characteristics obtained in the experiment are compared with those in simulation. Reasonable agreement is observed at all energies.

It is worth noting that tuning of the JETSET parameters for individual energy points allows one to reach better agreement between data and Monte Carlo than that achieved with the LUARLW generator in which the primary event multiplicity is a function of energy fixed beforehand and the distribution function in it is energy independent. However, at energies below 3 GeV tuning requires large efforts which are not adequate

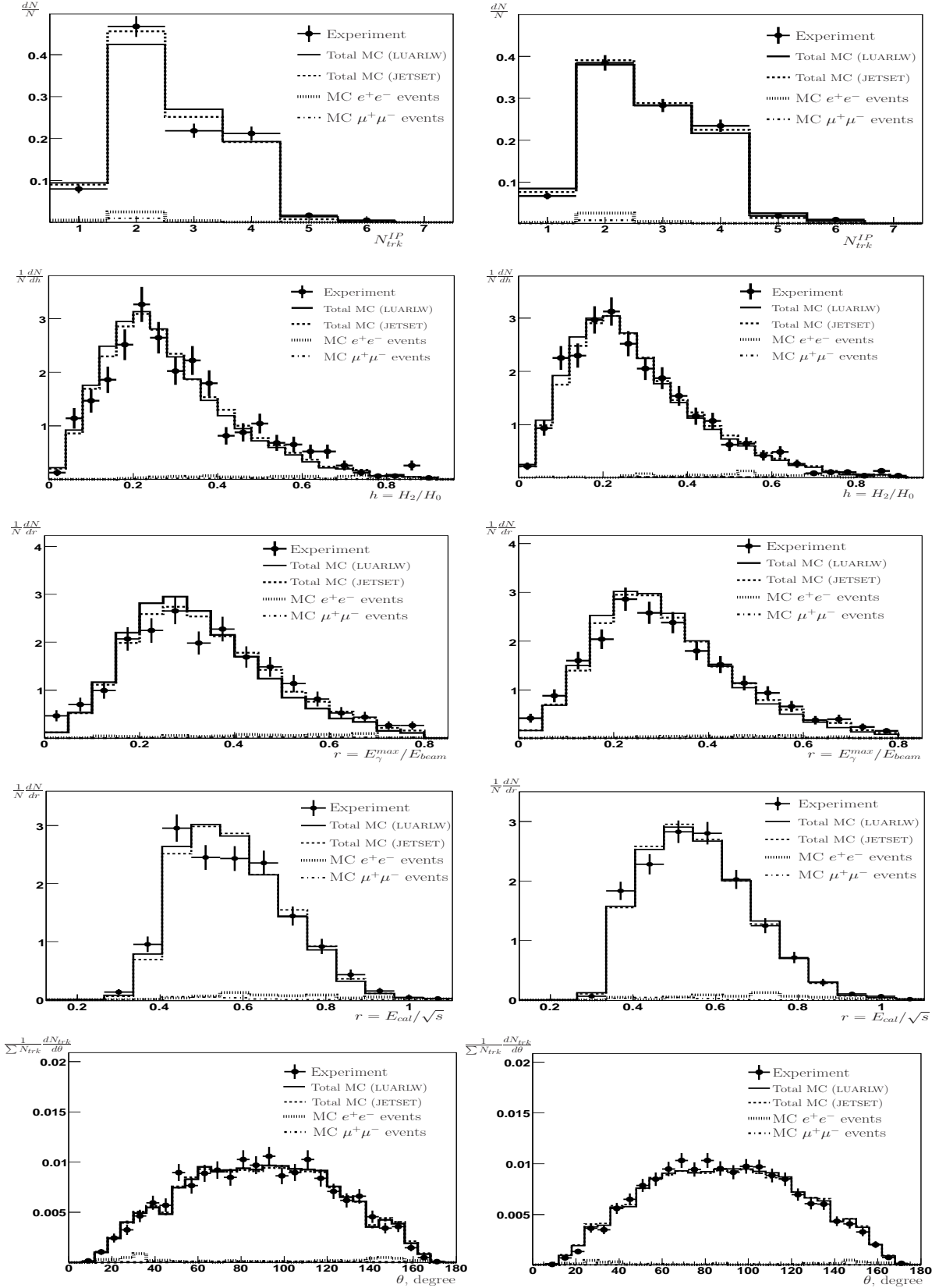


Figure 1: Properties of hadronic events produced in  $uds$  continuum at 1.94 GeV (left) and 2.14 GeV (right). Here,  $N$  is the number of events,  $H_2$  and  $H_0$  are Fox-Wolfram moments [30],  $E_\gamma^{\max}$  is energy of the most energetic photon,  $E_{\text{cal}}$  is energy deposited in the calorimeter,  $\theta$  is polar angle,  $N_{\text{trk}}$  is the number of tracks in event. The experimental distribution and two variants of MC simulation based on LUARLW and JETSET are plotted. All distributions are normalized to unity. Contributions of leptonic pair production are also presented.

for the statistically limited analysis. For this reason, unlike our work [11], it was done at some points only. The detection efficiencies obtained with the two event generators are listed in Table 3. The systematic uncertainties related to event simulation are discussed below in Section 5.2.

#### 4.3. Event selection and detection efficiencies

During the offline analysis, both experimental and simulated events pass the software event filter. This procedure allows us to reduce systematic inaccuracy due to trigger instabilities and uncertainties in the hardware thresholds. The software filter recomputes the PT and ST decisions with stringent conditions using a digitized response of the detector subsystems.

To suppress the machine background to an acceptable level, the following PT conditions were used by OR:

- signals from two or more non-adjacent scintillation counters ,
- signal from the LKr calorimeter ,
- coincidence of the signals from two CsI endcaps.

Signals from two particles with the angular separation  $\gtrsim 20^\circ$  should satisfy numerous ST conditions. The MC simulation yields the trigger efficiency of about 0.94 for continuum uds production.

Table 2: Selection criteria for hadronic events which were used by AND.

Variable	Allowed range
$N_{\text{trk}}^{\text{IP}}$	$\geq 1$
$E_{\text{obs}}$	$> 1.4 \text{ GeV}$ ( $> 1.3 \text{ GeV}$ if $E_{\text{beam}} < 1.05 \text{ GeV}$ )
$E_{\text{obs}} - E_{\gamma}^{\text{max}}$	$> 1.2 \text{ GeV}$ ( $> 1.1 \text{ GeV}$ if $E_{\text{beam}} < 1.05 \text{ GeV}$ )
$E_{\gamma}^{\text{max}}/E_{\text{beam}}$	$< 0.8$
$E_{\text{cal}}$	$> 0.55 \text{ GeV}$
$H_2/H_0$	$< 0.9$
$ P_z^{\text{miss}}/E_{\text{obs}} $	$< 0.6$
$E_{\text{LKr}}/E_{\text{cal}}$	$> 0.15$
$ Z_{\text{vertex}} $	$< 15.0 \text{ cm}$
$N_{\text{particles}} \geq 3$ or $\tilde{N}_{\text{trk}}^{\text{IP}} \geq 2$	

Selection criteria for multihadron events are listed in Table 2, and their description is provided below. In the Table  $N_{\text{trk}}^{\text{IP}}$  is the number of tracks from the interaction region defined by conditions  $\rho < 5 \text{ mm}$ ,  $|z_0| < 130 \text{ mm}$ , where  $\rho$  is the track impact parameter relative to the beam axis, and  $z_0$  is the coordinate of the closest approach point. The  $\tilde{N}_{\text{trk}}^{\text{IP}}$  is the number of tracks satisfying the conditions above with  $E/p$  less than 0.6, where  $E/p$  means the ratio of the energy deposited in the calorimeter to the measured momentum of the charged particle. The multiplicity  $N_{\text{particles}}$  is a sum of the number of charged tracks and the number of neutral particles detected in the calorimeters.

Table 3: Detection efficiency for the uds continuum in % (statistical errors only).

Point	$\epsilon_{\text{LUARLW}}$	$\epsilon_{\text{JETSET}}$	$\delta\epsilon/\epsilon$
1	$42.2 \pm 0.1$	$45.0 \pm 0.1$	$-6.6 \pm 0.3$
2	$47.2 \pm 0.1$	$46.0 \pm 0.1$	$-2.5 \pm 0.3$
3	$53.4 \pm 0.1$		
4	$52.5 \pm 0.1$	$51.3 \pm 0.1$	$-1.2 \pm 0.3$
5	$57.0 \pm 0.1$		
6	$61.6 \pm 0.1$		
7	$64.3 \pm 0.1$		
8	$66.7 \pm 0.1$		
9	$68.2 \pm 0.1$	$68.0 \pm 0.1$	$-0.2 \pm 0.2$
10	$70.3 \pm 0.1$	$70.6 \pm 0.1$	$+0.4 \pm 0.2$
11	$71.6 \pm 0.1$		
12	$73.0 \pm 0.1$		
13	$72.4 \pm 0.1$	$73.2 \pm 0.1$	$+1.1 \pm 0.2$

The observable energy  $E_{\text{obs}}$  is defined as a sum of the neutral cluster energies measured in the electromagnetic calorimeter and charged particle energies computed from the track momenta assuming pion masses. The observable energy cut and limitation on the ratio of the energy of the most energetic photon to the beam energy  $E_{\gamma}^{\text{max}}/E_{\text{beam}}$  suppress production of hadronic events at low center-of-mass energies through initial-state radiation and thus reduce the uncertainty of radiative corrections. The total calorimeter energy  $E_{\text{cal}}$  is defined as a sum of the energies of all clusters in the electromagnetic calorimeter. The cut on it suppresses the machine background. The cut on the ratio of Fox-Wolfram moments  $H_2/H_0$  is efficient for suppression of the  $e^+e^- \rightarrow e^+e^-\gamma$  background, that of cosmic rays and some kinds of the machine background. The background from two-photon and beam-gas events is suppressed by the cut on the ratio  $|P_z^{\text{miss}}/E_{\text{obs}}|$ , where  $P_z^{\text{miss}}$  is the z component of missing momentum. The background from beam-gas events was also suppressed by the cut on the ratio  $E_{\text{LKr}}/E_{\text{cal}}$  of the energy deposited in the LKr calorimeter and total calorimeter energy. The event vertex position  $Z_{\text{vertex}}$  is the weighted average of the  $z_0$ 's of the charged tracks. The cut on the  $|Z_{\text{vertex}}|$  suppresses background due to beam-gas, beam-wall and cosmic rays.

The muon system veto was required to reject cosmic rays background in the cases when more than two tracks did not cross the interaction region or the event arrival time determined by TOF relative to the bunch crossing was less than -7 ns or larger than 12 ns.

Compared with our previous work [11], we have introduced an additional condition on the difference of the observable energy and the energy of the most energetic photon that reduces the uncertainty of radiative corrections. At the same time, some of selection conditions were relaxed to increase the detection efficiency below 2.5 GeV.

The detection efficiency for hadronic events corresponding to the selection criteria described above is presented in Table 3

for thirteen data points at which the  $R$  ratio was measured. For six energy points it was determined using two versions of the event simulation.

#### 4.4. Luminosity determination

The integrated luminosity at each point was determined using Bhabha events detected in the LKr calorimeter in the polar angle range  $44^\circ < \theta < 136^\circ$ .

The criteria for  $e^+e^-$  event selection are listed below:

- two clusters, each with the energy above 20% of the beam energy and the angle between them exceeding  $162^\circ$ ,
- the total energy of these two clusters exceeds the beam energy,
- the calorimeter energy not associated with these two clusters does not exceed 30% of the total.

The tracking system was used only to reject the background from  $e^+e^- \rightarrow \gamma\gamma$  and  $e^+e^- \rightarrow \text{hadrons}$ .

#### 4.5. Physical background

To determine  $R$  values, we took into account the physical background contributions from the QED processes  $e^+e^- \rightarrow e^+e^-$  and  $e^+e^- \rightarrow \mu^+\mu^-$  which are summarized in Table 4.

The contributions of two-photon interactions were studied with a simulation of  $e^+e^- \rightarrow e^+e^-X$  events. We found that the contribution of two-photon events to the continuum cross section grows from 0.1% at 1.84 GeV to 0.3% at 3.05 GeV. The estimated uncertainty in the  $R$  value due to this contribution is less than 0.2%.

Table 4: The contribution of the physical background to the observed cross section in %.

Point	Process	
	$e^+e^-$	$\mu^+\mu^-$
1	$6.07 \pm 0.56$	$1.08 \pm 0.04$
2	$4.13 \pm 0.45$	$1.06 \pm 0.03$
3	$3.70 \pm 0.39$	$0.99 \pm 0.03$
4	$3.81 \pm 0.39$	$1.00 \pm 0.03$
5	$4.93 \pm 0.43$	$0.96 \pm 0.03$
6	$4.40 \pm 0.39$	$1.02 \pm 0.03$
7	$3.30 \pm 0.34$	$0.87 \pm 0.03$
8	$4.22 \pm 0.37$	$0.85 \pm 0.03$
9	$4.74 \pm 0.39$	$0.81 \pm 0.03$
10	$4.12 \pm 0.35$	$0.80 \pm 0.03$
11	$4.74 \pm 0.38$	$0.82 \pm 0.03$
12	$5.07 \pm 0.38$	$0.82 \pm 0.03$
13	$5.88 \pm 0.41$	$0.83 \pm 0.03$

#### 4.6. Correction for machine background

To estimate the contribution of residual machine background to the observed cross section, we use runs with separated  $e^+$  and  $e^-$  bunches.

The number of events that passed selection criteria in the runs with separated bunches was recalculated to the number of expected background events under the assumption that the background rate is proportional to the beam current and the measured vacuum pressure. As an alternative, we also performed analysis assuming that the background rate is proportional to the current only. The difference between the numbers of background events obtained with the two assumptions was considered as an uncertainty estimate at given energy point.

The background values and their uncertainties at each energy point are presented in Table 5.

Table 5: The residual machine background in % of the observed cross section

Point	Background, %	Point	Background, %
1	$1.4 \pm 0.5 \pm 0.4$	8	$0.4 \pm 0.4 \pm 0.2$
2	$1.4 \pm 0.5 \pm 0.2$	9	$1.2 \pm 0.6 \pm 0.2$
3	$1.2 \pm 0.4 \pm 0.2$	10	$1.8 \pm 0.7 \pm 0.3$
4	$1.6 \pm 0.7 \pm 0.2$	11	$1.2 \pm 0.4 \pm 0.2$
5	$2.1 \pm 0.8 \pm 0.2$	12	$2.1 \pm 0.9 \pm 0.2$
6	$1.3 \pm 0.6 \pm 0.2$	13	$1.3 \pm 0.5 \pm 0.2$
7	$0.6 \pm 0.6 \pm 0.6$		

#### 4.7. Radiative correction

The radiative correction factor was determined according to Eq. (4) using the compilation of the vacuum polarization data by the CMD-2 group [31] and the relation between  $R(s)$  and the hadronic part of the vacuum polarization  $\Pi_{\text{hadr}}(s)$ :

$$R(s) = -\frac{3}{\alpha} \text{Im} \Pi_{\text{hadr}}(s). \quad (5)$$

For each energy, the dependence of the detection efficiency on the energy radiated in the initial state was evaluated with the LUARLW and the MHG2000 generator, the latter developed by the CMD-3 collaboration [32, 33]. We apply the MHG2000 generator to simulate hadronic events below 1.84 GeV. This generator simulates about 30 various exclusive modes and approximately reproduces a real picture of  $e^+e^- \rightarrow \text{hadrons}$  below 2 GeV. The  $x$  dependencies of the detection efficiencies obtained with the LUARLW and MHG2000 generators for some energies are shown in Fig. 2.

Table 6 contains values of the radiative correction and their systematic uncertainties which are discussed in Sec. 5.3.

## 5. Systematic uncertainties and results

### 5.1. Systematic uncertainty of absolute luminosity determination

A summary of systematic uncertainties in the absolute luminosity determination with the LKr calorimeter is given in Table 7.

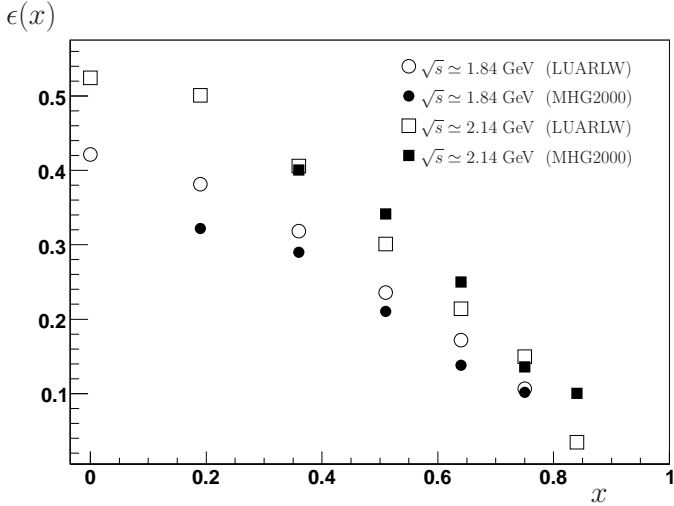


Figure 2: Hadronic detection efficiency versus variable  $x$  of Eq. (4) at 1.84 and 2.14 GeV.

Table 6: Radiative correction factor  $1 + \delta$

Point	$1 + \delta$	Point	$1 + \delta$
1	$1.0423 \pm 0.0208$	8	$1.0739 \pm 0.0054$
2	$1.0429 \pm 0.0156$	9	$1.0796 \pm 0.0054$
3	$1.0515 \pm 0.0126$	10	$1.0809 \pm 0.0054$
4	$1.0634 \pm 0.0106$	11	$1.0823 \pm 0.0054$
5	$1.0645 \pm 0.0096$	12	$1.0774 \pm 0.0054$
6	$1.0664 \pm 0.0075$	13	$1.0584 \pm 0.0053$
7	$1.0684 \pm 0.0064$		

The uncertainty related to the imperfect simulation of the calorimeter response was estimated by variation of relevant simulation parameters such as the geometrical factor controlling sensitivity to the energy loss fluctuations between calorimeter electrodes, the accuracy of the electronic channel calibration, etc.

The alignment of the LKr calorimeter with respect to the drift chamber was done with the help of cosmic tracks reconstructed in the tracking system. The direction of the beam line and interaction point were determined using the primary vertex distribution of multihadron events. The luminosity uncertainty due to inaccuracy of the alignment is less than 0.2%.

The difference in the polar angle resolutions observed in experiment and predicted by simulation causes an uncertainty in the luminosity measurement because events migrate into or out of the fiducial volume.

The uncertainty of the theoretical Bhabha cross section was estimated comparing the results obtained with the MCGPJ [26] and BHWIDE [34] event generators. It agrees with the errors quoted by the authors.

The background to the Bhabha process from the reactions  $e^+e^- \rightarrow \mu\mu(\gamma)$  and  $e^+e^- \rightarrow \gamma\gamma$  was estimated using MC simulation. It contributes less than 0.2% to the observed  $e^+e^-$  cross

Table 7: Systematic uncertainties of the luminosity determination.

Source	Uncertainty, %
Calorimeter response	0.7
Calorimeter alignment	0.2
Polar angle resolution	0.2
Cross section calculation	0.5
Background	0.1
MC statistics	0.1
Variation of cuts	0.8
Sum in quadrature	1.2

section for all energy points presented in Table 1. We also considered a contribution of residual machine background to Bhabha events which is about 0.1%. The residual luminosity uncertainty due to background does not exceed 0.1%.

In order to estimate the effect of other possible sources of uncertainty, we varied cuts within the fiducial region. The cuts on the polar angle were varied in a range much larger than the angular resolution, the variation in the Bhabha event count reaches 50%. The cut on the deposited energy was varied in the range of 50 – 80% of the c.m. energy. The variations discussed above correspond to a systematic uncertainty shown in Table 7.

These effects can occur due to the already considered sources and statistical fluctuations, nevertheless we add them in the total uncertainty to obtain conservative error estimates.

## 5.2. Uncertainty due to imperfect simulation of continuum

The imperfect simulation of the uds continuum contributes significantly to the systematic uncertainty in  $R$ . The maximal deviation of 1.2% is taken from Table 3 as the systematic uncertainty for the energy range 2.14-3.05 GeV. This estimate is consistent with our previous result for the LUARLW generator uncertainty of 1.3% obtained from continuum simulation above the  $J/\psi$  [11]. Below 2.14 GeV our estimations of this uncertainty are 2.5% for points 2 and 3 and 6.6% for point 1. These estimations were checked by the variation of selection criteria described in Section 5.4.

The contributions to the detection efficiency uncertainty due to imperfect simulation of the uds continuum are summarized in Table 8.

Table 8: Systematic uncertainties of the detection efficiency due to imperfect simulation of continuum.

Source	Uncertainty, %		
	Point 1	Points 2-3	Points 4-13
uds simulation	6.6	2.5	1.2
MC statistics	0.2	0.2	0.2
Sum in quadrature	6.6	2.5	1.2

### 5.3. Systematic uncertainty of the radiative correction

The main sources of systematic uncertainty associated with the radiative correction factor at each energy point are summarized in Table 9.

To estimate the uncertainty related to the accuracy of the vacuum polarization operator, we have compared two approximations to it. The first one was obtained by the CMD-2 group [31], the alternative one was extracted from the BES event generator [35]. The difference between them reaches 1.4% at the lowest energy point 1.84 GeV and drops down to 0.3% at the energy above 2.2 GeV.

The contribution denoted as  $\delta\varepsilon(s)$  is related to the uncertainty in the  $\varepsilon(s)$  dependence and obtained from the two alternative simulations below 1.84 GeV with the MHG2000 and LUARLW generators. The obtained difference in the  $1 + \delta$  value for each energy point is assigned as a systematic error due to  $\varepsilon(s)$  uncertainty.

The contribution  $\delta_{\text{calc}}$  is related to the interpolation uncertainty. It was evaluated comparing the results obtained using the linear interpolation and the quadratic one.

The estimated uncertainty in the radiative correction due to the  $R(s)$  uncertainty varies from 0.5% to 2.0% for the entire energy range.

Table 9: Systematic uncertainties of the radiative correction.

Point	Uncertainty, %				Total
	$\Pi$ approx.	$\delta\varepsilon(s)$	$\delta R(s)$	$\delta_{\text{calc}}$	
1	1.3	1.4	0.6	0.1	2.0
2	1.1	1.0	0.4	0.1	1.5
3	1.0	0.6	0.4	0.1	1.2
4	0.8	0.4	0.4	0.1	1.0
5	0.7	0.3	0.4	0.1	0.9
6	0.6	0.3	0.2	0.1	0.7
7	0.5	0.3	0.2	0.1	0.6
8	0.4	0.3	0.2	0.1	0.5
9	0.3	0.3	0.2	0.1	0.5
10	0.3	0.3	0.2	0.1	0.5
11	0.3	0.3	0.2	0.1	0.5
12	0.3	0.3	0.2	0.1	0.5
13	0.4	0.3	0.2	0.1	0.5

### 5.4. Detector-related uncertainties in $R$

The systematic uncertainties related to the efficiency of the track reconstruction were studied using Bhabha events and low-momentum cosmic tracks, and the appropriate correction was introduced in the MC simulation. The uncertainty of the correction gives the additional systematic uncertainty of about 0.5%.

The main source of the trigger efficiency uncertainty is that of the calorimeter thresholds in the secondary trigger. The estimate of about 0.2% was obtained varying the threshold in the software event filter. The inefficiency of the first level trigger

related to inefficiency of the time-of-flight counters is less than 0.2%.

The trigger efficiency and the event selection efficiency depend on the calorimeter response to hadrons. The uncertainty related to the simulation of nuclear interaction was estimated by comparison of the efficiencies obtained with the packages GHEISHA [36] and FLUKA [37] which are implemented in GEANT 3.21 [22]. The relative difference was about 0.4%.

To evaluate a systematic uncertainty related to the neutral events (no tracks in VD and three or more neutral particles) we add events that met the criteria which are listed in Table 10. This selection gives additional 0.7% of hadronic events and changes the average  $R$  within 0.2%, that serves as our estimate of the systematic uncertainty coming from neutral events.

Table 10: Selection criteria for neutral events which were used by AND.

Variable	Allowed range
$N_{\text{neutral particles}}^{\geq 3}$ and no tracks in VD	
$E_{\text{cal}}$	$> E_{\text{beam}}$
$E_{\text{cal}} - E_{\gamma}^{\text{max}}$	$> 1.2 \text{ GeV}$ ( $> 1.1 \text{ GeV}$ if $E_{\text{beam}} < 1.05 \text{ GeV}$ )
$H_2/H_0$	$< 0.9$
$E_{\text{LKr}}/E_{\text{cal}}$	$> 0.5$

The effect of other possible sources of the detector-related uncertainty was evaluated by varying the event selection cuts that are presented in Table 11. All observed  $R$  variations were smaller than their statistical errors and can originate from the already considered sources of uncertainties or the statistical fluctuations. Nevertheless, keeping the conservative estimate, we included them in the total uncertainty.

Table 11:  $R$  uncertainty due to variation of the selection criteria for hadronic events.

Variable	Range variation	$R$ variation in %
$E_{\text{obs}}$	$> 1.3 \div 1.7 \text{ GeV}$	0.3
$E_{\text{obs}} - E_{\gamma}^{\text{max}}$	$> 1.1 \div 1.4 \text{ GeV}$	0.3
$E_{\gamma}^{\text{max}}/E_{\text{beam}}$	$< 0.6 \div 0.9$	0.3
$E_{\text{cal}}$	$> 0.5 \div 0.8 \text{ GeV}$	0.2
$H_2/H_0$	$< 0.75 \div 0.92$	0.3
$ P_z^{\text{miss}}/E_{\text{obs}} $	$< 0.6 \div 0.8$	0.2
$E_{\text{LKr}}/E_{\text{cal}}$	$> 0.15 \div 0.25$	0.1
$ Z_{\text{vertex}} $	$< 12.0 \div 25.0 \text{ cm}$	0.2
Sum in quadrature		0.7

### 5.5. Energy determination uncertainty

During data collection at given energy point, the c.m. energy uncertainty was about 2 MeV. Meanwhile, the detection efficiency varied from 0.42 to 0.73 in the energy range of the experiment. That leads to inaccuracy of the detection efficiency

determination. Using linear efficiency interpolation between energy points, we estimated the contribution of the energy determination uncertainty to the  $R$  systematic error. It is about 0.1% for the entire energy range.

### 5.6. Results

A summary of the systematic uncertainties affecting the measurement of  $R$  is presented in Table 12.

Note that the contribution of the  $J/\psi$  resonance to the absolute  $R(s)$  value is not completely negligible for the upper point of the energy scan and amounts to  $6 \cdot 10^{-3}$ . This contribution was found analytically using "bare" parameters of the resonances, which were calculated based on the PDG data [38].

The obtained  $R$  values are listed in Table 13 and shown in Fig. 3.

Table 13: Measured values of  $R(s)$  with statistical and systematic uncertainties.

$\sqrt{s}$ , MeV	$R(s)$
1841.0	$2.226 \pm 0.139 \pm 0.158$
1937.0	$2.141 \pm 0.081 \pm 0.073$
2037.3	$2.238 \pm 0.068 \pm 0.072$
2135.7	$2.275 \pm 0.072 \pm 0.055$
2239.2	$2.208 \pm 0.069 \pm 0.053$
2339.5	$2.194 \pm 0.064 \pm 0.048$
2444.1	$2.175 \pm 0.067 \pm 0.048$
2542.6	$2.222 \pm 0.070 \pm 0.047$
2644.8	$2.220 \pm 0.069 \pm 0.049$
2744.6	$2.269 \pm 0.065 \pm 0.050$
2849.7	$2.223 \pm 0.065 \pm 0.047$
2948.9	$2.234 \pm 0.064 \pm 0.051$
3048.1	$2.278 \pm 0.075 \pm 0.048$

## 6. Summary

We have measured the  $R$  values at thirteen center-of-mass energies between 1.84 and 3.05 GeV. At most of the energy points, the achieved accuracy is about or better than 3.9% at the systematic uncertainty of 2.4%. The obtained  $R$  values are compatible with results of the previous experiments [1, 2, 4, 5, 6, 7] but provide more detailed information on the  $R(s)$  quantity in this energy range.

The weighted average  $R = 2.225 \pm 0.020 \pm 0.047$  agrees well with  $R_{\text{pQCD}} = 2.18 \pm 0.02$  calculated according to the pQCD expansion [39] for  $\alpha_s(m_\tau) = 0.333 \pm 0.013$  derived from the hadronic  $\tau$  decays [40]. The averaging was done by taking into account the partial correlation between systematic uncertainties for different energy points.

## Acknowledgments

We greatly appreciate the efforts of the staff of VEPP-4M to provide good operation of the complex during long term

experiments. The authors are grateful to V. P. Druzhinin and E. P. Solodov for useful discussions.

This work was supported by Russian Science Foundation under project N 14-50-00080. Work related to Monte Carlo generators was partially supported by Russian Foundation for Basic Research under grant 15-02-05674.

## References

- [1] P. A. Rapidis *et al.*, Phys. Rev. Lett. **39**, 526 (1977).
- [2] C. Bacci *et al.*, Phys. Lett. B **86**, 234 (1979).
- [3] M. Grilli *et al.*, Nuovo Cim. Lett. A **13**, 593 (1973).
- [4] B. Esposito *et al.*, Nuovo Cim. Lett. **30**, 65 (1981).
- [5] J. Z. Bai *et al.* (BES Collaboration), Phys. Rev. Lett. **84**, 594 (2000).
- [6] J. Z. Bai *et al.* (BES Collaboration), Phys. Rev. Lett. **88**, 101802 (2002).
- [7] M. Ablikim *et al.* (BES Collaboration), Phys. Lett. B **677**, 239 (2009).
- [8] N. Brambilla *et al.*, Eur. Phys. J. C **71**, 1534 (2011).
- [9] M. Davier *et al.*, Eur. Phys. J. C **71**, 1515 (2011).
- [10] K. Hagiwara *et al.*, J. Phys. G **38**, 085003 (2011).
- [11] V. V. Anashin *et al.*, Phys. Lett. B **753**, 533 (2016).
- [12] V. V. Anashin *et al.*, Stockholm 1998, EPAC 98\*, 400 (1998).
- [13] A. D. Bukin *et al.*, Absolute Calibration of Beam Energy in the Storage Ring. Phi-Meson Mass Measurement, Preprint IYF-75-64, 1975.
- [14] A. N. Skrinsky and Y. M. Shatunov, Sov. Phys. Usp. **32**, 548 (1989).
- [15] E. B. Levichev *et al.*, Phys. Usp. **57**, 66 (2014).
- [16] V. V. Anashin *et al.* (KEDR Collaboration), Phys. Lett. B **749**, 50 (2015).
- [17] V. E. Blinov *et al.*, ICFA Beam Dyn. Newslett. **48**, 195 (2009).
- [18] V. V. Anashin *et al.*, Phys. of Part. and Nucl. **44**, 657 (2013).
- [19] S. E. Baru *et al.*, Instrum. Exp. Tech. **54**, 335 (2011).
- [20] V. V. Anashin *et al.*, Phys. Lett. B **703**, 543 (2011).
- [21] E. A. Kuraev and V. S. Fadin, Sov. J. Nucl. Phys. **41**, 466 (1985).
- [22] GEANT – Detector Description and Simulation Tool CERN Program Library Long Writeup W5013.
- [23] Haiming Hu and An Tai, arXiv:hep-ex/0106017.
- [24] T. Sjostrand, M. Bengtsson, Comp. Phys. Comm. **43**, 367 (1987).
- [25] T. Sjostrand, S. Mrenna, P. Skands, PYTHIA 6.4 Physics and Manual, arXiv:hep-ph/0603175.
- [26] A. B. Arbuzov *et al.*, Eur. Phys. J. C **46**, 689 (2006).
- [27] F. A. Berends *et al.*, Comp. Phys. Comm. **40**, 285 (1986).
- [28] F. A. Berends *et al.*, Comp. Phys. Comm. **40**, 271 (1986).
- [29] V. A. Tayursky, S. I. Eidelman, Preprint IYaf 2000-78, Novosibirsk 2000 (in Russian).
- [30] G. C. Fox, S. Wolfram, Nucl. Phys. B **149**, 413 (1979).
- [31] S. Actis *et al.*, Eur. Phys. J. C **66**, 585 (2010).
- [32] H. Czyż *et al.*, Mini-Proc., 14th meeting of the Working Group on Rad. Corrections and MC Generators for Low Energies, arXiv:1312.0454.
- [33] H. Czyż *et al.*, Mini-Proc., 15th meeting of the Working Group on Rad. Corrections and MC Generators for Low Energies, arXiv:1406.4639.
- [34] S. Jadach, W. Placzek, B. F. L. Ward, Phys. Lett. B **390**, 298 (1997).
- [35] J. C. Chen *et al.*, Phys. Rev. D **62**, 034003 (2000).
- [36] H. C. Fesefeldt, Technical Report PITHA-85-02, III Physikalisches Institut, RWTH Aachen Physikzentrum, 5100 Aachen, Germany, Sep. 1985.
- [37] A. Fassò *et al.*, Talk at the Computing in High Energy and Nuclear Physics (CHEP03), arXiv:physics/0306162.
- [38] K. A. Olive *et al.* (PDG), Chin. Phys. C **38**, 090001 (2014).
- [39] P. A. Baikov *et al.*, Phys. Lett. B **714**, 62 (2012).
- [40] N. Brambilla *et al.*, Eur. Phys. J. C **74**, 2981 (2014).



Table 12:  $R$  systematic uncertainties (in %) assigned to each energy point.

	Point 1	Point 2	Point 3	Point 4	Point 5	Point 6	Point 7
Luminosity	1.2	1.2	1.2	1.2	1.2	1.2	1.2
Radiative correction	2.0	1.5	1.2	1.0	0.9	0.7	0.6
Continuum simulation	6.6	2.5	2.5	1.2	1.2	1.2	1.2
Track reconstruction	0.5	0.5	0.5	0.5	0.5	0.5	0.5
$l^+l^-$ contribution	0.6	0.5	0.4	0.4	0.4	0.4	0.3
$e^+e^-X$ contribution	0.2	0.2	0.2	0.2	0.2	0.2	0.2
Trigger efficiency	0.3	0.3	0.3	0.3	0.3	0.3	0.3
Nuclear interaction	0.4	0.4	0.4	0.4	0.4	0.4	0.4
Neutral events	0.2	0.2	0.2	0.2	0.2	0.2	0.2
Cuts variation	0.7	0.7	0.7	0.7	0.7	0.7	0.7
Machine background	0.6	0.5	0.4	0.7	0.8	0.6	0.8
Energy determination	0.1	0.1	0.1	0.1	0.1	0.1	0.1
Sum in quadrature	7.1	3.4	3.2	2.4	2.4	2.2	2.2
	Point 8	Point 9	Point 10	Point 11	Point 12	Point 13	
Luminosity	1.2	1.2	1.2	1.2	1.2	1.2	
Radiative correction	0.5	0.5	0.5	0.5	0.5	0.5	
Continuum simulation	1.2	1.2	1.2	1.2	1.2	1.2	
Track reconstruction	0.5	0.5	0.5	0.5	0.5	0.5	
$l^+l^-$ contribution	0.4	0.4	0.4	0.4	0.4	0.4	
$e^+e^-X$ contribution	0.2	0.2	0.2	0.2	0.2	0.2	
Trigger efficiency	0.3	0.3	0.3	0.3	0.3	0.3	
Nuclear interaction	0.4	0.4	0.4	0.4	0.4	0.4	
Neutral events	0.2	0.2	0.2	0.2	0.2	0.2	
Cuts variation	0.7	0.7	0.7	0.7	0.7	0.7	
Machine background	0.4	0.6	0.8	0.4	0.9	0.5	
Energy determination	0.1	0.1	0.1	0.1	0.1	0.1	
Sum in quadrature	2.1	2.2	2.2	2.1	2.3	2.1	

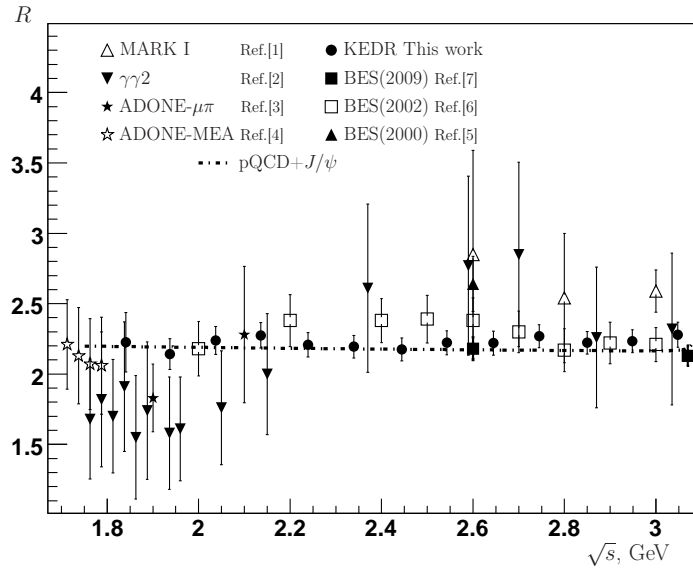


Figure 3: The quantity  $R$  versus the c.m. energy and the sum of the prediction of perturbative QCD and a contribution of the  $J/\psi$  resonance.